

Inverse obstacle scattering with limited-aperture data

Masaru Ikehata*, Esa Niemi[†], and Samuli Siltanen[‡]

August 25, 2011

Abstract

Inverse obstacle scattering aims to extract information about distant and unknown targets using wave propagation. This study concentrates on a two-dimensional setting using time-harmonic acoustic plane waves as incident fields and taking the obstacles to be sound-hard with smooth or polygonal boundary. Measurement data is simulated by sending one incident wave towards the area of interest and computing the far field pattern (1) on the whole circle of observation directions, (2) only in directions close to backscattering, and (3) only in directions close to forward-scattering. A variant of the enclosure method is introduced, based on applying the far field operator to an explicitly constructed density, yielding information about the convex hull of the obstacle. The numerical evidence presented suggests that the convex hull of obstacles can be approximately recovered from noisy limited-aperture far field data.

1 Introduction

Inverse obstacle scattering aims to extract information about distant and unknown targets using wave propagation. In this work we concentrate on the limited-aperture case of sending one incident wave towards the area of interest and measuring the scattered field in various directions. We introduce a novel

*Department of Mathematics, Graduate School of Engineering, Gunma University, Kiryu 376-8515, Japan, ikehata@math.sci.gunma-u.ac.jp

[†]Department of Mathematics and Statistics, University of Helsinki, Finland, esa.niemi@helsinki.fi

[‡]Department of Mathematics and Statistics, University of Helsinki, Finland, samuli.siltanen@helsinki.fi

computational algorithm (a variant of the *enclosure method*) for recovering the convex hull of a sound-hard obstacle from noisy limited-aperture far field data.

Let us formulate the direct problem. Assume that the scattering obstacle $D \subset \mathbb{R}^2$ is a bounded open set with Lipschitz boundary such that $\mathbb{R}^2 \setminus \overline{D}$ is connected. Denote by ν the unit outward normal to ∂D . Consider the scattering of the plane wave $e^{ikx \cdot d}$ with incident direction $d \in S^1$ and wave number $k > 0$. The scattered wave w is the unique solution of

$$\Delta w + k^2 w = 0 \quad \text{in } \mathbb{R}^2 \setminus \overline{D}, \quad (1.1)$$

$$\frac{\partial w}{\partial \nu} = -\frac{\partial}{\partial \nu} e^{ikx \cdot d} \quad \text{on } \partial D, \quad (1.2)$$

$$\lim_{r \rightarrow \infty} \sqrt{r} \left(\frac{\partial w}{\partial r} - ikw \right) = 0, \quad r = |x|. \quad (1.3)$$

The boundary condition (1.2) means that D is *sound-hard* and (1.3) is called the Sommerfeld radiation condition. For the uniqueness and existence of the solution see [29] for the potential theoretic approach and, for example, [10] for the variational approach. The above model arises for example as a cross-section of three-dimensional scattering from long cylindrical objects.

The *far field pattern* $F(\varphi; d, k)$ of w at the direction $\varphi \in S^1$ is defined as the leading term of the asymptotic expansion of w as $r \rightarrow \infty$ in the following sense:

$$w(r\varphi) = \frac{e^{ikr}}{\sqrt{r}} F(\varphi; d, k) + O\left(\frac{1}{r^{3/2}}\right). \quad (1.4)$$

The function $F(\varphi; d, k)$ models scattering data measured far from the obstacle in direction $\varphi \in S^1$. The direct problem is to determine F for a given obstacle D .

We consider the following inverse problem. Fix a wave number $k > 0$ and an incident direction $d \in S^1$. Measurement data is the knowledge of $F(\varphi; d, k)$ for φ ranging in an open and connected subset $\Gamma \subset S^1$ called *aperture*. The case that Γ is a proper subset of S^1 is referred to as the *limited-aperture case*; such cases arise for example from practical difficulties in surrounding the whole region of interest by sensors. If $\Gamma = S^1$, we are concerned with the *full-aperture case*. Define the *support function* of D by $h_D(\omega) := \sup_{x \in D} x \cdot \omega$, where $\omega \in S^1$ is an arbitrary direction, see Figure 1 for an illustration. Note that from precise knowledge of $h_D(\omega)$ for all $\omega \in S^1$ one can obtain the convex hull of D . The inverse problem is to determine $h_D(\omega)$ approximately for a given ω from measurement data corrupted by random noise.

Our approach for solving the inverse problem is based on the behaviour of the function

$$I_\omega(\tau) = \log \left| \int_{\Gamma} F(\varphi; d, k) g_N(-\varphi; \tau, k, \omega) d\sigma(\varphi) \right|, \quad \tau > 0, \quad (1.5)$$

where $d\sigma$ denotes arclength measure and the density function g_N is a truncation of a *formal solution* of the following integral equation of the first kind:

$$\int_{-\Gamma} e^{ikx \cdot \varphi} g(\varphi) d\sigma(\varphi) = e^{x \cdot (\omega + i\sqrt{\tau^2 + k^2} \omega^\perp)}, \quad (1.6)$$

where $x \in \mathbb{R}^2$ and $\omega^\perp = (\omega_2, -\omega_1)$. Note that the right-hand side of (1.6) satisfies the Helmholtz equation $\Delta v + k^2 v = 0$ in \mathbb{R}^2 and the left-hand side is called the Herglotz wave function with density g supported on $-\Gamma$. A combination of the unique continuation theorem for the Helmholtz equation and a comparison of the bound of both sides of (1.6) yields that for any nonempty open set U equation (1.6) for $x \in U$ is always *unsolvable*.

Throughout this paper we identify a point $\vartheta = (\vartheta_1, \vartheta_2) \in S^1$ with the complex number $\vartheta_1 + i\vartheta_2$ and denote it by the same symbol. The computation formula of the density g_N is explicitly given by the expansion

$$g_N(\varphi; \tau, k, \omega) = \sum_{m=0}^N \beta_m \varphi^m + \sum_{m=1}^N \beta_{-m} \bar{\varphi}^m, \quad \varphi \in -\Gamma, \quad (1.7)$$

where the set of coefficients β_m , $|m| \leq N$, is the unique solution of the linear system

$$G_N[\beta_{-N}, \dots, \beta_{-1}, \beta_0, \beta_1, \dots, \beta_N]^T = [\lambda^N, \dots, \lambda, 1, \lambda^{-1}, \dots, \lambda^{-N}]^T, \quad (1.8)$$

where the matrix G_N is element-wise given by

$$[G_N]_{m,j} = \int_{-\Gamma} \varphi^m \bar{\varphi}^j d\sigma(\varphi) = (\varphi^m, \bar{\varphi}^j)_{L^2(-\Gamma)} \quad (1.9)$$

with $m = N, \dots, -N$ and $j = -N, \dots, N$, and

$$\lambda = \frac{(\tau + \sqrt{\tau^2 + k^2}) \omega}{ik}. \quad (1.10)$$

Having defined the density g_N , we propose the following algorithm for solving the inverse problem for a finite collection of directions $\omega \in S^1$.

1. Choose parameters $N \geq 1$ and $0 \leq \tau_1 < \tau_2 < \tau_3$.

2. Compute $I_\omega(\tau_j)$ for $j = 1, 2, 3$ using (1.5).
3. Fit a line to the points $(\tau_j, I_\omega(\tau_j))$ in the sense of least squares. Denote the slope of the line by $\tilde{h}_D(\omega)$.
4. Approximate $h_D(\omega)$ by $\tilde{h}_D(\omega)$.

Note that the algorithm is computationally very inexpensive.

The *hypothesis* behind the above algorithm is: $\tilde{h}_D(\omega)$ is close to the value $h_D(\omega)$ of the support function. This hypothesis is based on the results in [18] by the first author. Therein, in the case that D is *polygonal*, i.e. D consists of a finite collection of polygons $\{D_j\}_{j=1}^m$ satisfying $\overline{D_j} \cap \overline{D_{j'}} = \emptyset$ for $j \neq j'$, two types of formulae are established. The first one of them shows that when $\Gamma = S^1$, the density g_N can be written in the simple form

$$g_N(\varphi; \tau, k, \omega) = \frac{1}{2\pi} \sum_{|m| \leq N} \left(\frac{\varphi}{\lambda}\right)^m, \quad (1.11)$$

and we have, with an appropriate choice of $\tau = \tau(N) \xrightarrow{N \rightarrow \infty} \infty$, that

$$\frac{1}{\tau} I_\omega(\tau) \longrightarrow h_D(\omega), \quad \text{as } N \rightarrow \infty. \quad (1.12)$$

The direction ω is assumed to be *regular* with respect to D , which means that the set $\{x \in \mathbb{R}^2 \mid x \cdot \omega = h_D(\omega)\} \cap \partial D$ consists of only one point (see Figure 1 for an illustration). Formula (1.12) suggests that for large τ we have

$$I_\omega(\tau) \approx h_D(\omega)\tau. \quad (1.13)$$

The second formula in [18] is for the limited-aperture case. However, in that case the density g_N is given implicitly by the *minimum norm solution* of the integral equation (1.6) in a bounded domain, the solution being based on Tikhonov regularization and Morozov discrepancy principle (see for example [7]). Using that density and the additional assumption that $h_D(\omega) > 0$, a formula similar to (1.12) for the limited-aperture case is established in [18]. We think that this also supports the hypothesis.

In this paper we present a derivation of the explicit density g_N given by (1.7). Moreover, we present numerical evidence suggesting that the proposed algorithm yields approximate convex hulls of obstacles from noisy limited-aperture data. The method seems to work reasonably well also in the case of obstacles with smooth boundary. Note that in this case the asymptotic behaviour of $I_\omega(\tau)$ as $\tau \rightarrow \infty$ has not yet been studied.

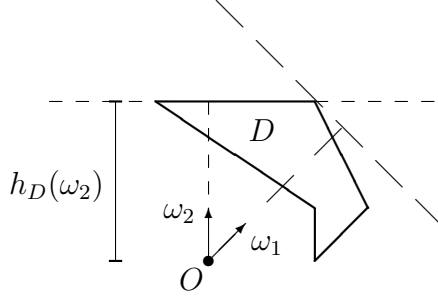


Figure 1: A polygonal obstacle D , a regular direction ω_1 with respect to D , a non-regular direction ω_2 with respect to D , and the value $h_D(\omega_2)$ of the support function.

Many approaches for solving inverse obstacle scattering problems have been proposed and tested numerically, and they can be roughly divided into direct and iterative methods. For the large body of literature concerning iterative methods we refer to [8] and references therein. Direct approaches, such as the one proposed here, include the *linear sampling method* of Colton-Kirsch [4, 9, 2], the *probe method* of Ikehata [11, 13], the *factorization method* of Kirsch [23, 24], the *enclosure method* of Ikehata [14, 15], the *scattering support approach* of Kusiak and Sylvester [27, 28], the *singular sources method* of Potthast [33, 32], and the *no response test* of Luke and Potthast [30]. See [3, 8] for reviews of the various methods. See also [25] for a comparison of some of the methods above, [19] for a survey on the probe and enclosure methods for inverse obstacle scattering problems and [22] for several results on uniqueness, stability and numerical methods in inverse problems for partial differential equations.

How does the present approach compare to other direct methods making use of only one incident direction? The *no response test* [30] aims to decide whether D is contained in a test domain D_t by studying the following functional with a parameter $\epsilon > 0$:

$$L_\epsilon(D_t) := \sup \left\{ \left| \int_{\Gamma} F(\varphi; d, k) g(-\varphi) d\sigma(\varphi) \right| : \sup_{y \in D_t} \left| \int_{-\Gamma} e^{iky \cdot \varphi} g(\varphi) d\sigma(\varphi) \right| \leq \epsilon \right\}.$$

In the case of sound-soft obstacles, i.e. the Neumann boundary condition (1.2) replaced with Dirichlet boundary condition $w(x) = -e^{ikx \cdot d}$ on ∂D , it is shown in [30] that, if $D \subset D_t$, then $L_\epsilon(D_t) = 0$, and if $\overline{D} \cap \overline{D_t} = \emptyset$, then $L_\epsilon(D_t) = \infty$. However, as pointed out in Remark 3.3 of [30], this does not give us the complete characterization whether $D \subset D_t$ or not. A numerical algorithm based on the above facts is proposed and numerically studied in

[30]. It is known that the no response test together with the *range test* [35] provides a criterion to test the analytic extensibility of the field. See [34] for this view point and further information.

The convex scattering support in [27] is the smallest convex set supporting a source that can produce a given far field pattern on the *whole* unit circle. They introduced a test that tells us if the far field could have been produced by a source located within a specific domain. It is a test on the behaviour of the m th Fourier coefficient of the far field pattern, that is, the behaviour of

$$\int_{S^1} F(\varphi; d, k) \varphi^m d\sigma(\varphi), \quad m = 0, \pm 1, \pm 2, \dots$$

as $|m| \rightarrow \infty$. A numerical algorithm for finding the convex scattering support is introduced and numerically studied in [35]. Compared to the scattering support approach, the proposed enclosure method yields complementary information since the scattering support of D and the convex hull of D are not subsets of each other in general.

This paper is organized as follows. In Section 2 we present a derivation of the density given by (1.7) and provide some remarks on the hypothesis. In Section 3 we describe computational methods related to the simulation of data and to the inversion algorithm. Numerical results are presented in Section 4, and we discuss and conclude our results in Section 5.

2 Background of the method

We present in Subsection 2.1 an argument for the derivation of the density g_N given by (1.7) with coefficients satisfying (1.8). In Subsection 2.2 we discuss the hypothesis by reviewing the main result in [18] and provide some remarks concerning the asymptotic behaviour of $I_\omega(\tau)$ as $\tau \rightarrow \infty$ in the case of non-polygonal obstacles.

2.1 A derivation of the limited-aperture density

The argument for the derivation employs an idea in [18] reducing the integral equation (1.6) to another integral equation via the Vekua transform [36, 37] which maps harmonic functions into solutions of the Helmholtz equation.

By [31] the Bessel function of order $m = 0, \pm 1, \pm 2, \dots$ is given by

$$J_m(z) = \left(\frac{z}{2}\right)^m \sum_{n=0}^{\infty} \frac{(-1)^n}{n! \Gamma(n+1+m)} \left(\frac{z}{2}\right)^{2n}.$$

The Vekua transform in two dimensions takes the form

$$T_k v(x) = v(x) - \frac{k|x|}{2} \int_0^1 v(tx) J_1(k|x|\sqrt{1-t}) \frac{dt}{\sqrt{1-t}},$$

where v is an arbitrary harmonic function in \mathbb{R}^2 .

The argument is based on the following facts about two exponential solutions of the Helmholtz equation.

(i) Define the harmonic function $e_\omega(x; \tau, k)$ in the whole space by

$$e_\omega(x; \tau, k) = e^{(\tau - \sqrt{\tau^2 + k^2})\bar{\omega}(x_1 + ix_2)/2} + e^{(\tau + \sqrt{\tau^2 + k^2})\omega(x_1 - ix_2)/2} - 1.$$

Then, the Vekua transform of $e_\omega(x; \tau, k)$ coincides with function $e^{x \cdot (\omega + i\sqrt{\tau^2 + k^2}\omega^\perp)}$. See [18] for the proof.

(ii) The Vekua transform of the harmonic function

$$e^{ik\bar{\varphi}(x_1 + ix_2)/2} + e^{ik\varphi(x_1 - ix_2)/2} - 1$$

coincides with $e^{ikx \cdot \varphi}$. This is a consequence of the Jacobi-Anger expansion

$$e^{ikx \cdot \varphi} = \sum_{m=0}^{\infty} (i\bar{\varphi})^m J_m(kr) e^{im\theta} + \sum_{m=0}^{\infty} (i\varphi)^m J_m(kr) e^{-im\theta} - J_0(kr), \quad x = (r \cos \theta, r \sin \theta)$$

and the fact that $T_k : r^m e^{\pm im\theta} \mapsto (2/k)^m m! J_m(kr) e^{\pm im\theta}$.

Using (i) and (ii) we reduce the construction of formal solution of (1.6) to that of the integral equation

$$\int_{-\Gamma} \{e^{ik\bar{\varphi}(x_1 + ix_2)/2} + e^{ik\varphi(x_1 - ix_2)/2} - 1\} g(\varphi) d\sigma(\varphi) = e_\omega(x; \tau, k). \quad (2.1)$$

We find a density having the form

$$g(\varphi) = \sum_{m=0}^{\infty} \beta_m \varphi^m + \sum_{m=1}^{\infty} \beta_{-m} \bar{\varphi}^m, \quad \varphi \in -\Gamma, \quad (2.2)$$

Using the power series expansion of the both sides of (2.1), we see that if one chooses $\beta_m, m = 0, \pm 1, \pm 2, \dots$ in such a way that

$$\begin{aligned} \left(\frac{ik}{2}\right)^m \int_{-\Gamma} \varphi^m g(\varphi) d\sigma(\varphi) &= \left(\frac{(\tau + \sqrt{\tau^2 + k^2})\omega}{2}\right)^m, \quad m = 1, 2, 3, \dots, \\ \left(\frac{ik}{2}\right)^m \int_{-\Gamma} \bar{\varphi}^m g(\varphi) d\sigma(\varphi) &= \left(\frac{(\tau - \sqrt{\tau^2 + k^2})\bar{\omega}}{2}\right)^m, \quad m = 0, 1, 2, \dots, \end{aligned}$$

then g satisfies (2.1) exactly. Using (1.10) the above equations can be rewritten as

$$\int_{-\Gamma} \varphi^m g(\varphi) d\sigma(\varphi) = \lambda^m, \quad m = 1, 2, 3, \dots, \quad (2.3)$$

$$\int_{-\Gamma} \bar{\varphi}^m g(\varphi) d\sigma(\varphi) = \lambda^{-m}, \quad m = 0, 1, 2, \dots \quad (2.4)$$

Substituting (2.2) into (2.3) and (2.4), we obtain

$$\lambda^m = \sum_{j=0}^{\infty} \beta_j \int_{-\Gamma} \varphi^m \varphi^j d\sigma(\varphi) + \sum_{j=1}^{\infty} \beta_{-j} \int_{-\Gamma} \varphi^m \bar{\varphi}^j d\sigma(\varphi) \quad (2.5)$$

$$\lambda^{-m} = \sum_{j=0}^{\infty} \beta_j \int_{-\Gamma} \bar{\varphi}^m \varphi^j d\sigma(\varphi) + \sum_{j=1}^{\infty} \beta_{-j} \int_{-\Gamma} \bar{\varphi}^m \bar{\varphi}^j d\sigma(\varphi). \quad (2.6)$$

Since $\varphi^{-1} = \bar{\varphi}$ on S^1 , from a truncation of (2.5) and (2.6) we get (1.8). Note that the matrix G_N in (1.8) is the Gram matrix for the linearly independent functions φ^m , $-N \leq m \leq N$ in $L^2(-\Gamma)$ and thus invertible. Therefore, the coefficients β_m are uniquely determined for $-N \leq m \leq N$ by (1.8). In computer implementation it is convenient and straightforward to solve (1.8) numerically.

2.2 Some remarks on the hypothesis

As already mentioned in Introduction, the hypothesis behind the proposed algorithm is motivated by [18] where the first author established an explicit formula based on a simpler version of the enclosure method [16, 17]. The formula yields information about the convex hull of D provided that D is *polygonal*. Let us next state the formula precisely. Denote by B_R the open disc of radius R centered at the origin.

Theorem 2.1 ([18]). *Assume that the obstacle D is polygonal and $\bar{D} \subset B_R$. Let ω be regular with respect to D , and let β_0 be the unique positive solution of $\frac{2}{e}s + \log s = 0$. Assume that β satisfies $0 < \beta < \beta_0$ and that $\{\tau(N)\}_{N \in \mathbb{N}}$ is an arbitrary sequence of positive numbers satisfying*

$$\tau(N) = \frac{\beta N}{eR} + O(1)$$

as $N \rightarrow \infty$. Then, assuming that the density function g_N is given by (1.11), the following formula holds:

$$\lim_{N \rightarrow \infty} \frac{1}{\tau(N)} \log \left| \int_{S^1} F(\varphi; d, k) g_N(-\varphi; \tau(N), k, \omega) d\sigma(\varphi) \right| = h_D(\omega). \quad (2.7)$$

For non-polygonal obstacles the validity of (2.7) is an open problem. To understand the central part of the problem let us make a review of the proof of Theorem 2.1. The density g_N given by (1.11) with some $\tau(N)$ satisfies, as $N \rightarrow \infty$,

$$\begin{aligned} v_{g_N}(x) &\equiv \int_{S^1} e^{ikx \cdot \varphi} g_N(\varphi) d\sigma(\varphi) \\ &= e^{x \cdot (\tau(N)\omega + i\sqrt{\tau(N)^2 + k^2}\omega^\perp)} + O(e^{-R\tau(N)} N^{-\infty}), \quad x \in \bar{B}_R, \end{aligned}$$

together with its first order derivatives. This together with the formula [6]

$$\int_{S^1} F(\varphi; d, k) g_N(-\varphi) d\sigma(\varphi) = -\frac{e^{i\pi/4}}{\sqrt{8\pi k}} \int_{\partial B_R} \left(\frac{\partial w}{\partial \nu} v_{g_N} - \frac{\partial v_{g_N}}{\partial \nu} w \right) d\sigma,$$

where ν is the unit outward normal relative to B_R enables us to connect the left-hand side above with the asymptotic behaviour of the integral

$$\int_{\partial B_R} \left(\frac{\partial w}{\partial \nu} v_\tau - \frac{\partial v_\tau}{\partial \nu} w \right) d\sigma \Big|_{\tau=\tau(N)}$$

where $v_\tau(x) = e^{x \cdot (\tau\omega + i\sqrt{\tau^2 + k^2}\omega^\perp)}$. If D is polygonal and ω is regular with respect to D , then by [17], for some positive constants μ and A one gets

$$\tau^\mu e^{-\tau h_D(\omega)} \left| \int_{\partial B_R} \left(\frac{\partial w}{\partial \nu} v_\tau - \frac{\partial v_\tau}{\partial \nu} w \right) d\sigma \right| \rightarrow A \quad (2.8)$$

as $\tau \rightarrow \infty$, and by the above reasoning one obtains (2.7) from (2.8).

Thus the key point is to analyze the asymptotic behaviour of the integral of the left-hand side of (2.8) as $\tau \rightarrow \infty$. For general obstacles this remains open, however, one can state the following fact.

Proposition 2.1. *Assume that there exist $\lambda, \mu \in \mathbb{R}$ and $A > 0$ such that*

$$\tau^\mu e^{-\tau\lambda} \left| \int_{\partial B_R} \left(\frac{\partial w}{\partial \nu} v_\tau - \frac{\partial v_\tau}{\partial \nu} w \right) d\sigma \right| \rightarrow A.$$

Then it must hold that $\lambda \leq h_D(\omega)$.

Proof. Integration by parts gives the expression

$$\tau^\mu e^{-\tau\lambda} \int_{\partial B_R} \left(\frac{\partial w}{\partial \nu} v_\tau - \frac{\partial v_\tau}{\partial \nu} w \right) d\sigma = -\tau^\mu e^{-\tau(\lambda - h_D(\omega))} \int_{\partial D} w e^{-\tau h_D(\omega)} \frac{\partial v_\tau}{\partial \nu} d\sigma. \quad (2.9)$$

Since $x \cdot \omega \leq h_D(\omega)$ and $|\partial v_\tau / \partial \nu| \leq \sqrt{2\tau^2 + k^2} e^{\tau x \cdot \omega}$ for all $x \in \partial D$, the integral of the right-hand side has a bound $O(\tau)$ as $\tau \rightarrow \infty$. Thus if

$\lambda > h_D(\omega)$, then the right-hand side of (2.9) converges to zero and thus $A = 0$. Contradiction. \square

At the present time we do not know whether the equality $\lambda = h_D(\omega)$ or even the assumption in Proposition 2.1 holds for non-polygonal obstacles. We leave this for a future research.

3 Computational methods

In this section we describe the computational methods that yield the numerical results presented in Section 4. We begin by explaining the method for solving the direct scattering problem, that is, for generating the far field pattern data. We then proceed to propose our method for the inverse problem of extracting information about the convex hull of an obstacle from the knowledge of the far field pattern on an aperture $\Gamma \subset S^1$.

3.1 Simulation of scattering data

Our method for computing the far field pattern data is based on layer potential representation and boundary integral equations, for details see for example [5]. More precisely, the solution of the Neumann problem (1.1)–(1.3) can be written in the form

$$w(x) = \int_{\partial D} \Phi(x-y)f(y)ds(y),$$

where the density f is a solution of the boundary integral equation

$$f(x) - 2 \int_{\partial D} \frac{\partial \Phi(x-y)}{\partial \nu(x)} f(y)ds(y) = 2 \frac{\partial}{\partial \nu} e^{ikx \cdot d}, \quad x \in \partial D. \quad (3.1)$$

We remark that equation (3.1) may fail to be uniquely solvable for certain choices of D and k , which can lead to numerical difficulties. In the numerical examples below we avoid such situations simply by trial-and-error. Above Φ is the fundamental solution of the Helmholtz equation, that is

$$\Phi(x) = \frac{i}{4} H_0^{(1)}(k|x|),$$

where $H_0^{(1)}$ is the Hankel function of the first kind and order zero [31]. This layer potential representation together with the asymptotic form (1.4) and with the asymptotic properties of $H_0^{(1)}$ imply that the far field pattern can be written as

$$F(\varphi; d, k) = \frac{e^{i\pi/4}}{\sqrt{8\pi k}} \int_{\partial D} e^{-ik\varphi \cdot y} f(y)ds(y). \quad (3.2)$$

Hence, to compute F we first solve the density f from (3.1) and then use (3.2).

It remains to explain how we approximate the integrals in (3.1) and in (3.2). To do this, we choose a piecewise smooth parametrization $x(t)$, $t \in [0, 2\pi]$ for the boundary curve ∂D and discretize it into $2n$ points as follows:

$$x_j = x(t_j), \quad t_j = \frac{j\pi}{n}, \quad j = 0, 1, \dots, 2n - 1.$$

We note that by the properties of the Hankel functions the kernel of the integral operator in (3.1) can be written as

$$\begin{aligned} K(t, s) &:= \frac{\partial \Phi(x(t) - x(s))}{\partial \nu(x(t))} \\ &= -\frac{ik}{4} H_1^{(1)}(k|x(t) - x(s)|) \frac{\nu(x(t)) \cdot (x(t) - x(s))}{|x(t) - x(s)|} |x'(s)|, \end{aligned}$$

where the Hankel function $H_1^{(1)}$ has an (integrable) singularity at zero. To overcome the numerical problems caused by this singularity, we follow [26] and write the kernel in the form

$$K(t, s) = K_1(t, s) \ln \left(4 \sin^2 \frac{t-s}{2} \right) + K_2(t, s),$$

where

$$K_1(t, s) := \frac{k}{4\pi} J_1(k|x(t) - x(s)|) \frac{\nu(x(t)) \cdot (x(t) - x(s))}{|x(t) - x(s)|} |x'(s)|$$

and

$$K_2(t, s) := K(t, s) - K_1(t, s) \ln \left(4 \sin^2 \frac{t-s}{2} \right)$$

turn out to be analytic with diagonal terms

$$K_1(t, t) = 0, \quad K_2(t, t) = \frac{1}{4\pi} \nu(x(t)) \cdot x''(t).$$

Similarly to [26] we use the following quadrature rules to approximate the resulting integrals:

$$\begin{aligned} \int_0^{2\pi} K_1(t, s) \ln \left(4 \sin^2 \frac{t-s}{2} \right) f(x(s)) ds &\approx \sum_{j=0}^{2n-1} R_j(t) K_1(t, t_j) f(x_j), \\ \int_0^{2\pi} K_2(t, s) f(x(s)) ds &\approx \frac{\pi}{n} \sum_{j=0}^{2n-1} K_2(t, t_j) f(x_j), \end{aligned}$$

where the first quadrature with weights

$$R_j(t) = -\frac{2\pi}{n} \sum_{m=1}^{n-1} \frac{\cos(m(t-t_j))}{m} - \frac{\pi}{n^2} \cos(n(t-t_j))$$

is obtained by replacing $K_1(t, \cdot)f(x(\cdot))$ by its trigonometric interpolation polynomial and then integrating exactly, whereas the second quadrature is simply the trapezoidal rule. Now, using the above quadratures, the discretized version of the integral equation (3.1) can be written as

$$f(x_i) - 2 \sum_{j=0}^{2n-1} \left[R_j(t_i)K(t_i, t_j) + \frac{\pi}{n} K_2(t_i, t_j) \right] f(x_j) = 2 \frac{\partial}{\partial \nu(x(t_i))} e^{ikx_i \cdot d},$$

$i = 0, 1, \dots, 2n-1$. We solve this system of linear equations with an iterative method, such as GMRES, for $[f(x_1), f(x_2), \dots, f(x_{2n-1})]^T$ and evaluate then the far field pattern at observation directions $\varphi_\ell \in S^1$, $\ell = 1, 2, \dots, p$ by approximating the integral in (3.2) by trapezoidal rule:

$$F(\varphi_\ell; d, k) \approx \frac{e^{i\pi/4}}{\sqrt{8\pi k}} \frac{\pi}{n} \sum_{j=0}^{2n-1} e^{-ik\varphi_\ell \cdot x_j} f(x_j) |x'(t_j)|.$$

To simulate the case of noisy data we add 1% Gaussian random noise

$$\frac{0.01}{\sqrt{2}} (\epsilon_1 + i\epsilon_2) \max_{\varphi_\ell} |F(\varphi_\ell; d, k)|$$

to each value $F(\varphi_\ell; d, k)$ of the far field pattern. Here $\epsilon_1, \epsilon_2 \sim \mathcal{N}(0, 1)$ are normally distributed random numbers with mean zero and unit variance. We shall refer to this data as *noisy data*, while the data without added noise are called *noise-free data*.

We remark that adding 1% noise to the far-field pattern does not necessarily correspond to 1% data in practical applications. In practice one usually has available point values of the total field with certain error level, and the relationship of such data to the idealized concept of far-field pattern requires a specific application-dependent study.

3.2 Computation of the support function

The main challenge in the numerical implementation of the enclosure method is estimating the value of the support function $h_D(\omega)$ without using large values of parameters N and τ . Increasing N and τ rapidly lead to large values of $|g_N|$, which causes numerical instability especially with noisy data.

Following the ideas presented in [21, 1, 20], we estimate $h_D(\omega)$ as follows. We choose some $N \in \mathbb{N}$ and a few values $\tau_1, \tau_2, \tau_3 \geq 0$ of τ and compute the corresponding quantities

$$I_\omega(\tau_j) = \log \left| \int_{\Gamma} F(\varphi; d, k) g_N(-\varphi; \tau_j, k, \omega) d\sigma(\varphi) \right|, \quad j = 1, 2, 3,$$

where the integral over Γ is approximated by the sum

$$\frac{\text{length}(\Gamma)}{p} \sum_{\ell=1}^p F(\varphi_\ell; d, k) g_N(-\varphi_\ell; \tau_j, k, \omega)$$

with p uniformly distributed vectors φ_ℓ on Γ . Then, motivated by (2.7), we fit a straight line to the points $(\tau_j, I_\omega(\tau_j))$ in a least-squares sense and approximate $h_D(\omega)$ by the slope of this line. Hence, we propose recovering the convex hull of D approximately by repeating this algorithm for a finite collection of directions $\omega \in S^1$.

To evaluate the indicator function $I_\omega(\tau)$ we compute the values of g_N by using the limited-aperture density (1.7). To do this, we first form the matrix G_N and the vector λ in equation (1.8) and solve for the coefficients β . Since the matrix G_N becomes ill-conditioned for small apertures Γ (see below), we use truncated singular value decomposition with truncation level 10^{-6} to regularize the equation.

The fact that the matrix G_N becomes ill-conditioned for small apertures can be seen as follows. Consider the case when $\Gamma = \{-e^{i\theta} : |\theta| < \epsilon\}$ with $0 < \epsilon < \pi$. Since

$$\int_{-\Gamma} \varphi^m \varphi^j d\sigma(\varphi) = \begin{cases} \frac{2 \sin(m+j)\epsilon}{m+j}, & \text{if } m+j \neq 0, \\ 2\epsilon, & \text{if } m+j = 0, \end{cases}$$

we see that G_N has the form

$$2\epsilon \begin{pmatrix} 1 & \frac{\sin \epsilon}{\epsilon} & \cdots & \frac{\sin(2N-1)\epsilon}{(2N-1)\epsilon} & \frac{\sin 2N\epsilon}{2N\epsilon} \\ \frac{\sin \epsilon}{\epsilon} & 1 & \cdots & \frac{\sin(2N-2)\epsilon}{(2N-2)\epsilon} & \frac{\sin(2N-1)\epsilon}{(2N-1)\epsilon} \\ \vdots & \vdots & \vdots & \vdots & \vdots \\ \frac{\sin(2N-1)\epsilon}{(2N-1)\epsilon} & \frac{\sin(2N-2)\epsilon}{(2N-2)\epsilon} & \cdots & 1 & \frac{\sin \epsilon}{\epsilon} \\ \frac{\sin 2N\epsilon}{2N\epsilon} & \frac{\sin(2N-1)\epsilon}{(2N-1)\epsilon} & \cdots & \frac{\sin \epsilon}{\epsilon} & 1 \end{pmatrix}.$$

From this we see that when ϵ is small, $G_N \approx 2\epsilon(\mathbf{1})$, where $(\mathbf{1})$ denotes $(2N + 1) \times (2N + 1)$ matrix whose all elements are equal to one. Hence, the matrix G_N becomes nearly singular for small apertures.

We remark that the proposed algorithm consists of numerical integration quadratures, solution of a (small) system of linear equations and standard least squares fitting. Therefore, the inversion method is inexpensive computationally.

Finally a comment related to the regularity of the directions ω . In [20] a so-called rejection rule for non-regular directions was proposed. This was to eliminate the negative effect to reconstructions caused by corrupted values of the support function in non-regular directions. Same type of rule can be applied to the algorithm presented above. However, in this paper we use no rejection rule but compute and use the values of the support function for non-regular directions as well.

In the following section we illustrate the proposed method and the choice of the parameters N and τ with numerical examples.

4 Numerical results

In this section we present a set of numerical results of the proposed implementation of the enclosure method.

In all the examples the far field pattern data was generated by using the method described in Section 3.1 with 600 discretization points on the boundary ∂D of the obstacle. To achieve rapid convergence, for polygonal obstacles we applied appropriate changes of variables yielding more dense grid near the corners than elsewhere on ∂D . The wave number is $k = 1$ in all examples. Other parameters including the number of discretization points on the aperture Γ are reported for each result separately.

The reconstructions were computed as explained in Section 3.2, and they are shown as follows: gray areas in the plots depict the reconstructed convex hulls of the obstacles, and the correct boundaries of the obstacles are indicated by black curves. The directions ω were chosen to be 16 uniformly distributed vectors on S^1 unless otherwise stated.

Reconstructions in the first two figures, Figures 2 and 3, make use of the far field pattern data on the full aperture $\Gamma = S^1$, while in the last two figures, Figures 4 and 5, the aperture Γ is only $1/2$ and $1/4$ of the unit circle S^1 , respectively. Figure 2 illustrates with a simple example how the method works. In Figure 3 reconstructions computed from both noise-free and noisy data for a smooth and a polygonal obstacle are presented. Figures 4 and 5 demonstrate reconstructions from limited-aperture far field data in forward-

and back-scattering type settings.

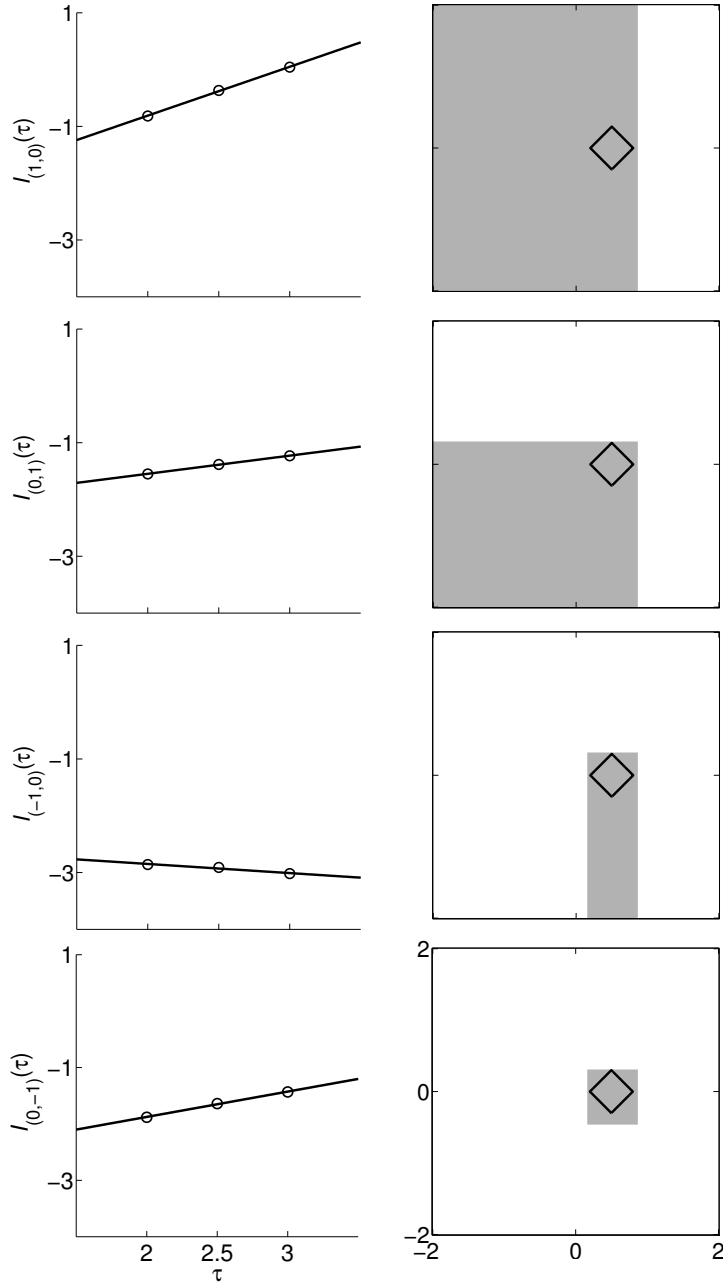


Figure 2: Step-by-step illustration of the method; each $\omega \in S^1$ and the slope of the corresponding fitted line determine a half-plane in which the (sound-hard) obstacle lies. *Left*: straight lines fitted to the points $(\tau, I_\omega(\tau))$ (the points indicated by circles in the plots) for four directions $\omega = (1, 0), (0, 1), (-1, 0), (0, -1)$. *Right*: reconstruction after each step. Gray areas in the plots show the computed convex hulls and black curves indicate the correct boundary of the obstacle. In this example $N = 6$, and the incident direction is $d = (1, 0)$. The aperture Γ here is the whole unit circle discretized uniformly into 512 points.

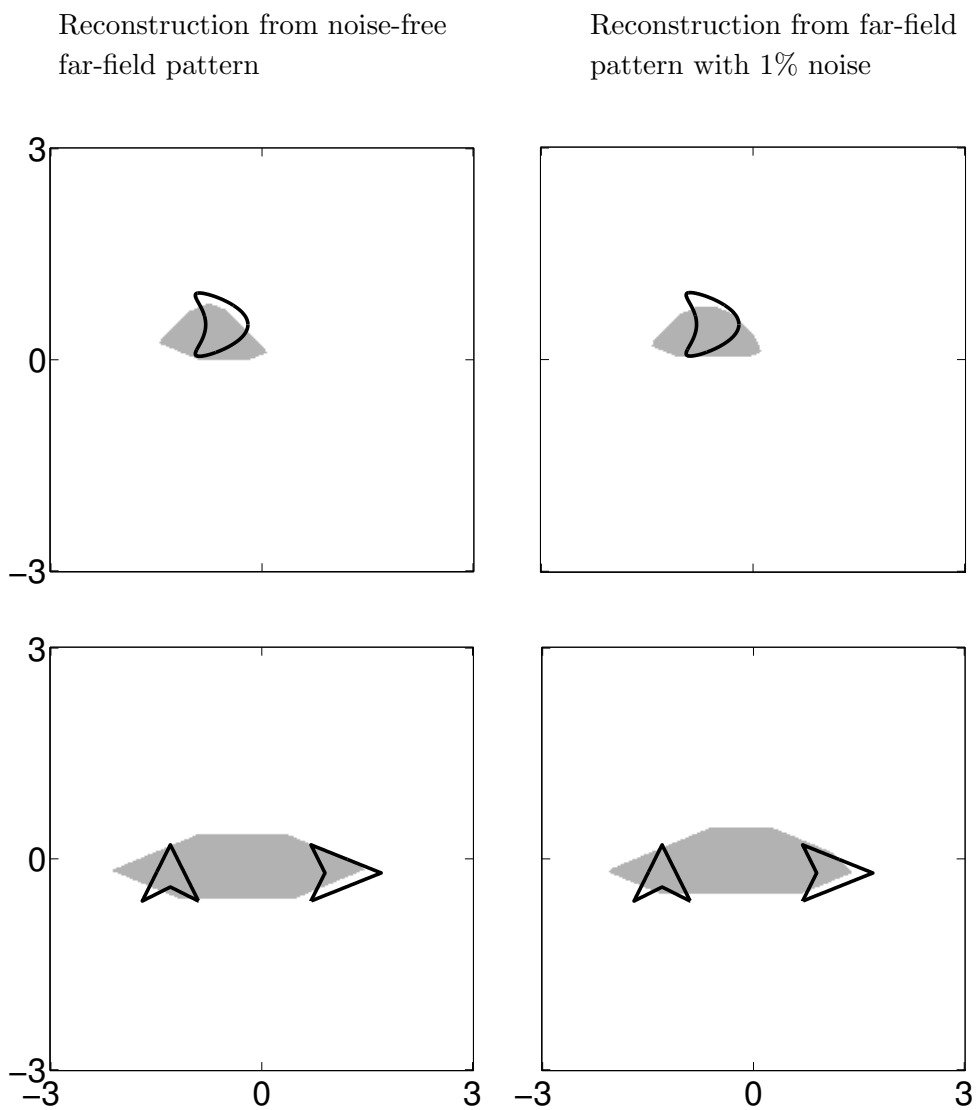


Figure 3: Reconstructions from noise-free and noisy far-field patterns corresponding to two sound-hard obstacles. Gray areas in the plots depict the computed convex hulls, and black curves indicate the correct boundaries of the obstacles. The parameters are $N = 4$ and $\tau = 0, 0.5, 1$ on the first row, and $N = 5$ and $\tau = 0, 0.5, 1$ on the second row. The incident direction is $d = (1, 0)$. The aperture Γ here is the whole unit circle discretized uniformly into 512 points.

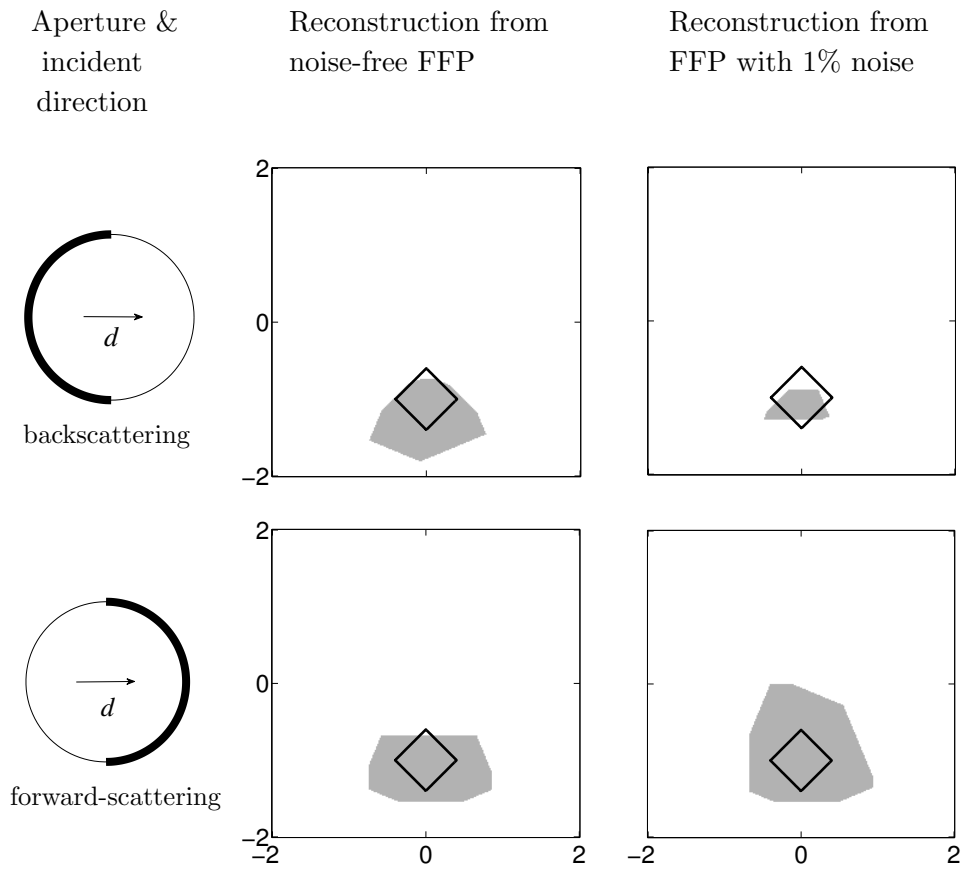


Figure 4: Polygonal sound-hard obstacle and limited-aperture data. First column: the apertures $\Gamma \subset S^1$ indicated by the bold parts of the circles, and the incident direction $d = (1,0)$ shown inside the circles. Second and third column: reconstructions for each aperture from ideal and noisy data, respectively. Gray areas depict the computed convex hulls, and black curves indicate the correct boundary of the obstacle. The number of discretization points on Γ is 256. The values of the parameters are $N = 4$ and $\tau = 0, 0.5, 1$.

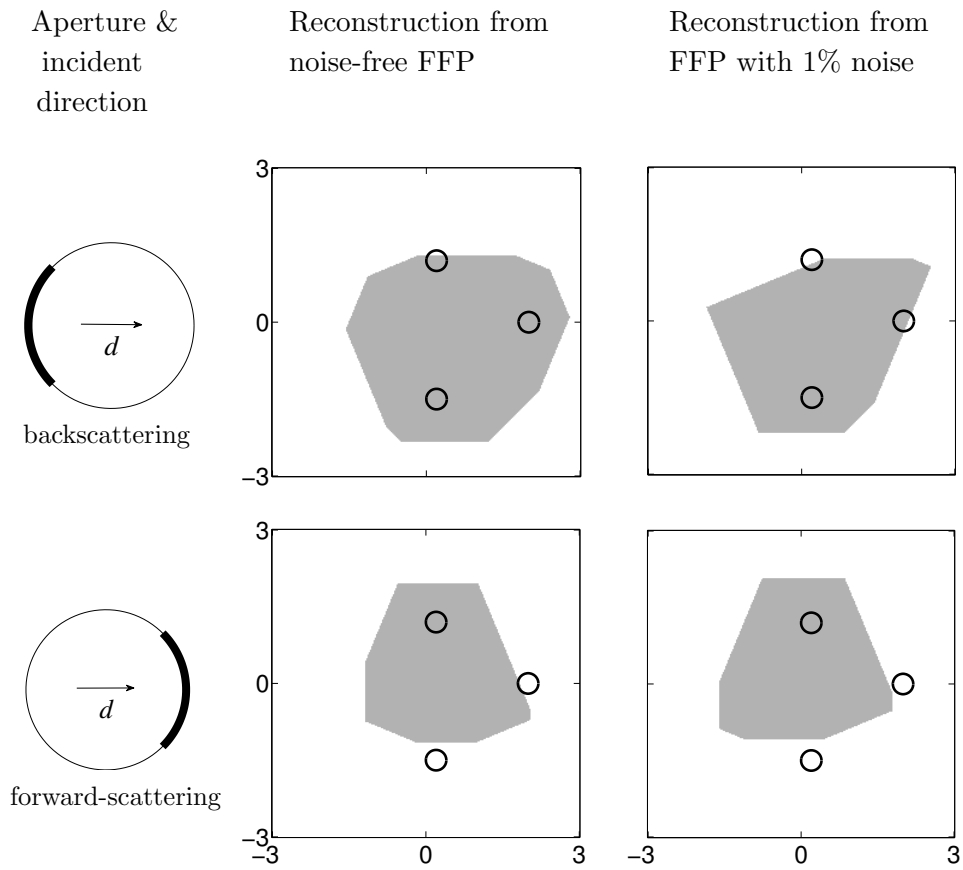


Figure 5: Smooth sound-hard obstacle and limited-aperture data. First column: the apertures $\Gamma \subset S^1$ indicated by the bold parts of the circles, and the incident direction $d = (1,0)$ shown inside the circles. Second and third column: reconstructions for each aperture from ideal and noisy data, respectively. Gray areas depict the computed convex hulls, and black curves indicate the correct boundary of the obstacle. The number of discretization points on Γ is 128. The values of the parameters are $N = 4$ and $\tau = 0, 0.5, 1$.

5 Discussion

We propose a new variant of the enclosure method for two-dimensional inverse obstacle scattering. The method is designed for limited-aperture data consisting of the far field pattern for a fixed wave number, one incident direction and possibly limited-aperture observations.

The method was examined through numerical experiments. This paper should be viewed as an initial feasibility study since the method is tested for the first time, and furthermore, some of the example obstacles are not covered by the theoretical analysis of the algorithm.

To simulate measurement data, the far field patterns of various smooth and polygonal obstacles were computed approximately adapting the method from [26], see Section 3.1 above. Comparing the numerical far field patterns achieved at different discretization levels suggests that the relative point-wise absolute error in the noise-free far field patterns is significantly less than 1%. We simulated noisy measurements by adding 1% relative random error to the far field patterns.

The results shown in Figure 3 are computed from full-aperture data for a one-component smooth obstacle and a two-component polygonal obstacle. The reconstructed convex hulls and actual convex hulls are not subsets of each other: there are some incorrectly recovered areas (false positives) as well as parts of the actual convex hull that are not seen in the reconstruction (false negatives). However, the location and area of the reconstructed set is close to those of the actual convex hull. Also, our experiments with different realizations of the random noise (not shown in figures) suggest that the reconstructions do not change much with the noise.

The results shown in Figures 4 and 5 concern the case of limited-aperture data, both in backscattering and forward-scattering geometries. These cases are more sensitive to noise than the full-aperture case, as expected. The location and area of the reconstructed set vary significantly, and there is a considerable amount of both false negative areas and false positive areas in the results. Studies with many realizations of the random noise component suggest that generally there is a recovered set (of some possibly incorrect shape) near the obstacle, and most of the time the center of the obstacle is included in the reconstruction. The backscattering case is more sensitive to noise in this respect than the forward-scattering case: for some realizations of noise the reconstruction is almost empty.

The method seems to be somewhat sensitive to the choice of the parameters N and τ as well. As a rule of thumb, the larger the distance between the origin and the convex hull of the obstacle, the larger values of N have to be used to obtain reasonable reconstructions. And when N is large, τ values

must be small to avoid numerical instability. This implies that reconstructing obstacles located far away from the origin is difficult. If the obstacle lies close to the origin and this is known *a priori*, optimal reconstruction is obtained by using smaller value of N and larger values of τ .

On the other hand, the regularity of directions ω seems not to be very critical provided that the values of τ are small. However, a simple way to reduce possible negative effects of non-regular directions is to give the reconstruction as a function obtained by summing characteristic functions of half-planes:

$$\sum_j \chi_{H_j}(x), \quad H_j = \{x \in \mathbb{R}^2 \mid x \cdot \omega_j < \tilde{h}_D(\omega_j)\}.$$

Showing this function as a grayscale image yields intuitive graphical information on the probability of points belonging to the convex hull of the unknown obstacle.

In conclusion, the limited-aperture enclosure method provides computationally inexpensive means for recovering approximate convex hulls of sound-hard obstacles from limited-aperture scattering data. Some application-dependent tuning of parameters is to be expected. In the case of full-aperture data, the location and area of the convex hull are robustly recovered, but the recovered shape of the convex hull is not reliable. For limited-aperture data the results typically only indicate the general location of the obstacle.

6 Acknowledgements

We thank Fioralba Cakoni, David Colton and Nuutti Hyvönen for helpful discussions. Also, we are grateful to the anonymous referees for their constructive criticism on the manuscript. MI was partially supported by Grant-in-Aid for Scientific Research (C)(No. 21540162) of Japan Society for the Promotion of Science. The work of EN and SS was financially supported by the Academy of Finland (Center of Excellence programme 213476 and Computational Science Research Programme, project 134868 and project 141094). In addition, SS was supported by Grant-in-Aid for JSPS Fellows (No. 00002757) of the Japan Society for the Promotion of Science. This project was partially conducted at the Mathematical Sciences Research Institute, Berkeley, whose hospitality is gratefully acknowledged.

References

- [1] Bruhl M and Hanke M 2000, *Numerical implementation of two noniterative methods for locating inclusions by impedance tomography*, Inverse Problems **16**, 1029–1042.
- [2] Cakoni F, Colton D and Monk P 2011, *The Linear Sampling Method in Inverse Electromagnetic Scattering*, SIAM.
- [3] Colton D, Coyle J and Monk P 2000, *Recent Developments in Inverse Acoustic Scattering Theory*, SIAM Review **42**, 369–414.
- [4] Colton D and Kirsch A 1996, *A simple method for solving inverse scattering problems in the resonance region*, Inverse Problems **12**, 383–393.
- [5] Colton D and Kress R 1983, *Integral equation methods in scattering theory*, John Wiley & Sons.
- [6] Colton D and Kress R 1995, *Eigenvalues of the far field operator for the Helmholtz equation in an absorbing medium*, SIAM J. Appl. Math. **55**, 1724–1735.
- [7] Colton D and Kress R 1998, *Inverse acoustic and electromagnetic scattering theory*, Springer.
- [8] Colton D and Kress R 2006, *Using fundamental solutions in inverse scattering*, Inverse Problems **22**, R49–R66
- [9] Colton D and Monk P 1998, *A linear sampling method for the detection of leukemia using microwaves* SIAM J. Appl. Math. **58**, 926–941
- [10] Hettlich F 1994, *On the uniqueness of the inverse conductivity scattering problem for the Helmholtz equation*, Inverse Problems **10**, 129–144.
- [11] Ikehata M 1998, *Reconstruction of an obstacle from the scattering amplitude at a fixed frequency*, Inverse Problems **14**(1998), 949–954.
- [12] Ikehata M 1999, *Reconstruction of a source domain from the Cauchy data*. Inverse Problems **15**, 637–645.
- [13] Ikehata M 1999, *Reconstruction of obstacle from boundary measurements*, Wave Motion **30**, 205–223.
- [14] Ikehata M 1999, *How to draw a picture of an unknown inclusion from boundary measurements. Two mathematical inversion algorithms*, J. Inv. Ill-Posed Problems **7**, 255–271.

- [15] Ikehata, M 2000, *Reconstruction of the support function for inclusion from boundary measurements*, J. Inv. Ill-Posed Problems **8**, 367–378.
- [16] Ikehata, M 2003, *Complex geometrical optics solutions and inverse crack problems*, Inverse Problems **19**, 1385–1405.
- [17] Ikehata M 2004, *Inverse scattering problems and the enclosure method*, Inverse Problems **20**, 533–551.
- [18] Ikehata M 2005, *The Herglotz wave function, the Vekua transform and the enclosure method*, Hiroshima Math. J. **35**, 485–506.
- [19] Ikehata M 2010, *The probe and enclosure methods for inverse obstacle scattering problems. The past and present.*, New developments of functional equations in Mathematical Analysis, *RIMS Kôkyûroku*, No.1702, 1–22.
- [20] Ikehata M and Ohe T 2002, *A numerical method for finding the convex hull of polygonal cavities using the enclosure method*, Inverse Problems **18**, 111–124.
- [21] Ikehata M and Siltanen S 2000, *Numerical method for finding the convex hull of an inclusion in conductivity from boundary measurements*, Inverse Problems **16**, 1043–1052.
- [22] Isakov V 2006, *Inverse problems for partial differential equations* (Second Edition), Springer, New York.
- [23] Kirsch A 1998, *Characterization of the shape of a scattering obstacle using the spectral data of the far field operator*, Inverse Problems **14**, 1489–1512.
- [24] Kirsch A 2000, *New characterizations of solutions in inverse scattering theory*, Appl. Anal. **76**, 319–350.
- [25] Kirsch A and Grinberg N 2008, *The factorization method for inverse problems*, Oxford University Press, Oxford.
- [26] Kress R 1995, *On the numerical solution of a hypersingular integral equation in scattering theory*, Journal of Computational and Applied Mathematics **61**, 345–360.
- [27] Kusiak S and Sylvester J 2003, *Scattering support*, Comm. Pure Appl. Math. **56**, 1525–1548.

- [28] Kusiak S and Sylvester J 2003, *The convex scattering support in a background medium* SIAM J. Math. Anal. **36**, 1142–1158
- [29] Liu C 1995, *The Helmholtz equation on Lipschitz domains*, Preprint.
- [30] Luke D and Potthast R 2003, *The no response test—a sampling method for inverse scattering problems*, SIAM J. Appl. Math. **63**, 1292–1312.
- [31] Olver F W J 1974, *Asymptotics and special functions*, Academic Press, New York and London.
- [32] Potthast R 1998, *A point source method for inverse acoustic and electromagnetic obstacle scattering problems*, IMA J. Appl. Math. **61**, 119–140.
- [33] Potthast R 2000, *Stability estimates and reconstructions in inverse scattering using singular sources*, J. Comp. Appl. Math. **114**, 247–274.
- [34] Potthast R 2007, *On the convergence of the no response test*, SIAM J. Math. Anal., vol. 38, No. 6, 1808–1824.
- [35] Potthast R, Sylvester J and Kusiak S 2003, *A ‘range test’ for determining scatterers with unknown physical properties*, Inverse Problems **19**, 533–547.
- [36] Vekua, I., *On the solution of the equation $\Delta u + \lambda^2 u = 0$* , Bull. Acad. Sci. Georgian SSR, 3(1942), 307-314.
- [37] Vekua, I., *Inversion of an integral transformation and some of its properties*, Bull. Acad. Sci. Georgian SSR, 6(1945), 177-183.